Military Technical College
Kobry El-Kobbah,
Cairo, Egypt

9th International Conference on
Electrical Engineering
ICEENG 2014

COMPARATIVE SYNTHESIS OF UAV FLIGHT CONTROL IN PRESENCE OF ACTUATORS AND SENSORS DYNAMICS

M. Korany*, A. M. Youssef** and G. El-sheikh***

ABSTRACT:

Unmanned aerial vehicles (UAVs) have become a hot research topic in the worldwide due to their great potential in numerous military and civil implementations. This motivated ever-increasing attraction of designing UAV flight control systems to achieve robust stability and acceptable performance across specified flight envelopes. Therefore, this paper is devoted to design an adequate flight control system for stabilizing a fixed wing (**Aerosonde**) UAV. To achieve this objective, successive activities are considered including the derivation of aircraft nonlinear equations of motion and tailoring them for use on the underlying aircraft. The dynamics of both sensors and actuators are integrated to the nonlinear model in a modular Simulink model. Trimming the nonlinear model for steady-state flight and extracting the linearized models for the UAV are then considered. Two different design techniques are used for designing the UAV flight controller; the classical PID and the fuzzy controllers. A comparative synthesis between these controllers is performed for specific altitude and speed commands. Simulation results showed acceptable responses except that the fuzzy approach yields better time responses and disturbance rejection than the classical one.

Keywords: UAV**,** PID and Fuzzy control

Nomenclature

e_0,e_x,e_y,e_z	Quaternions	$V_N\ V_E\ V_D$	Velocity in navigation frame
p,q,r	Angular rates	A_x, A_y,A_z	Acceleration in body frame
J_{prop}	Propeller moment of inertia	u,v,w	Velocity in body frame
J_{eng}	Engine moment of inertia:	L,D,Y	Lift, Drag and Side Force
ω	propeller rotation speed	l,m,n	Roll, Pitch and yaw Moment
ρ	Air density	M_{prop}	Propulsion system moments
R	Propeller radius	M_{eng}	Engine moments
C_T	Propeller coefficient of thrust	F_{prop}	Propulsion system forces
C_P	Propeller coefficient of power	$c_{1\ldots\ldots}c_9$	Inertia coefficients

1- Introduction

The arena of UAVs has for many years been dominated by civilian and military industries since they are indispensable for various applications where human intervention is considered difficult or dangerous. One of the important endeavors in UAV related research is the design of its flight control system to achieve robust stability and acceptable performance across specified flight envelope in presence of actuators and sensor uncertainties. The first step in designing such control system is to create a mathematical model of the aircraft. For an aerospace vehicle, developing a mathematical model requires knowledge of the physical characteristics such as weight, mass properties and aerodynamic parameters. The flight simulation is an essential part of guidance, navigation, and control design and development. The extensive use of simulation for saving time and prevent a perhaps crash of the aerial vehicle in flight test.

2. Model of Aerosonde UAV

2.1 Mathematical Model of Aerosonde UAV

A generalized full six degrees of freedom nonlinear mathematical model of a rigid symmetric aircraft can be written as follows:

$$\dot{u} = r \cdot v - q \cdot w + A_X \quad (1)$$

$$\dot{v} = -r \cdot u + p \cdot w + A_Y \quad (2)$$

$$\dot{w} = q \cdot u - p \cdot v + A_Z \quad (3)$$

$$\dot{p} = (c_1 \cdot r + c_2 \cdot p) \cdot q + c_3 \cdot l + c_4 \cdot n \quad (4)$$

$$\dot{q} = c_5 \cdot u \cdot r - c_6 \cdot (p^2 - r^2) + c_7 \cdot m \quad (5)$$

$$\dot{r} = (c_8 \cdot p - c_2 \cdot r) \cdot q + c_4 \cdot l + c_9 \cdot n \quad (6)$$

$$\dot{lat} = V_N / (R_m + h) \quad (7)$$

$$\dot{long} = V_E / ((R_n + h) \cdot \cos\phi) \quad (8)$$

$$\dot{h} = -V_D \quad (9)$$

$$\dot{e}_0 = \left(-p \cdot e_X - q \cdot e_Y - r \cdot e_Z\right) \Big/ \left(2 \cdot \sqrt{e_0{}^2 + e_X{}^2 + e_Y{}^2 + e_Z{}^2}\right) \tag{10}$$

$$\dot{e}_X = \left(p \cdot e_0 + r \cdot e_Y - q \cdot e_Z\right) \Big/ \left(2 \cdot \sqrt{e_0{}^2 + e_X{}^2 + e_Y{}^2 + e_Z{}^2}\right) \tag{11}$$

$$\dot{e}_Y = \left(q \cdot e_0 - r \cdot e_X + p \cdot e_Z\right) \Big/ \left(2 \cdot \sqrt{e_0{}^2 + e_X{}^2 + e_Y{}^2 + e_Z{}^2}\right) \tag{12}$$

$$\dot{e}_Z = \left(r \cdot e_0 + q \cdot e_X - p \cdot e_Y\right) \Big/ \left(2 \cdot \sqrt{e_0{}^2 + e_X{}^2 + e_Y{}^2 + e_Z{}^2}\right) \tag{13}$$

These equations represent the forces, moment, navigation, and kinematic equations. The mathematical model involves the propulsion system which includes a piston engine and a fixed-pitch propeller. The propulsion model is represented by a simple internal combustion engine model based on look-up tables of engine parameters.

$$\left(J_{eng} + J_{prop}\right) \cdot \dot{\omega} = M_{eng} + M_{\Pr op} \tag{14}$$

Where

$$F_{\Pr op} = \frac{4}{\pi^2} \rho R^4 \omega^2 C_T \quad , \quad M_{\Pr op} = -\frac{4}{\pi^3} \rho R^5 \omega^2 C_P$$

For the longitudinal flight control system, the airspeed V_t, the pitch angle θ, the pitch-rate q, and the altitude h are monitored:

$$V_t = \sqrt{u^2 + v^2 + w^2} \tag{15}$$

$$\theta = \sin^{-1}\left(2 \cdot \left(e_Y \cdot e_0 - e_X \cdot e_Z\right)\right) \tag{16}$$

According to the aerodynamic stability and control derivatives associated to the Aerosonde UAV [8], the nonlinear aircraft model is linearized about the trim condition (straight and level flight: u = 23m/s, h = 100m, $\beta = \phi = 0$). The linearized model is then integrated with the models of the actuators and sensors.

2.2 Actuators Modeling

The actuators in the Aerosonde UAV are flap, elevator, ailerons, rudder and thrust. Characteristics of UAV actuators are shown in Table-2.

Table-2: Characteristics of Aerosonde UAV actuators.

Actuator	Position limit δ_{max} *(deg)*	Slew rate limit $\dot{\delta}_{\max}$ *(deg/s)*
Flap	-1:+15	±40
Elevator	±15	±40
Aileron	±15	±40
Rudder	±20	±1.15
Throttle	10% : 100%	-

Flap:

$$\frac{\delta_F}{\delta_{F_d}} = \frac{\omega_n^2}{S^2 + 2\zeta\omega_n S + \omega_n^2} = \frac{30.74^2}{S^2 + 2(0.509)(30.74)S + 30.74^2} \tag{17}$$

Elevator:
$$\frac{\delta_E}{\delta_{E_d}} = \frac{\omega_n^2}{S^2 + 2\zeta\omega_n S + \omega_n^2} = \frac{30.74^2}{S^2 + 2(0.509)(30.74)S + 30.74^2} \quad (18)$$

Aileron:
$$\frac{\delta_A}{\delta_{A_d}} = \frac{\omega_n^2}{S^2 + 2\zeta\omega S + \omega_n^2} = \frac{75^2}{S^2 + 2(0.59)(75)S + 75^2} \quad (19)$$

Rudder:
$$\frac{\delta_R}{\delta_{R_d}} = \frac{\omega_n^2}{S^2 + 2\zeta\omega S + \omega_n^2} = \frac{72.1^2}{S^2 + 2(0.69)(72.1)S + 72.1^2} \quad (20)$$

Thrust actuator:
$$\frac{\delta_{th}}{\delta_{th_d}} = \frac{1/T}{S + 1/T} = \frac{1/0.2666}{\mathrm{S} + 1/0.2666} \quad (21)$$

2.3 Sensor Modeling

The sensors involved in the simulation are the accelerometers, the gyroscopes, the air data senors (angle of attack probe, sideslip vane, altitude and velocity sensors), the compass and the GPS.

2.3.1 The Three-Axis Accelerometer Modeling

The three-axis accelerometer model implements an accelerometer on each axis.

$$\overline{A}_{meas} = \overline{A}_{imeas} \times \overline{A}_{SFCC} + \overline{A}_{bias} + noise \quad (22)$$

Where $\overline{A}_{meas}$ is measured accelerations, $\overline{A}_{SFCC}$ is a 3-by-3 matrix of scaling factors on the diagonal and misalignment terms in the non-diagonal, $\overline{A}_{bias}$ are the biases, $\overline{\omega}_b$ are body-fixed angular rates, $\dot{\overline{\omega}}_b$ are body-fixed angular accelerations and $\overline{d}$ is the lever arm and the ideal measured accelerations:

$$\overline{A}_{imeas} = \overline{A}_b + \overline{\omega}_b \times \left(\overline{\omega}_b \times \overline{d}\right) + \dot{\overline{\omega}}_b \times \overline{d} - \overline{g} \quad (23)$$

2.3.2 The Three-Axis Gyroscope Modeling

The three-axis gyroscope model implements a gyroscope on each axis.

$$\overline{\omega}_{meas} = \overline{\omega}_b \times \overline{\omega}_{SFCC} + \overline{\omega}_{bias} + Gs \times \overline{\omega}_{gsens} + noise \quad (24)$$

where $\overline{\omega}_{meas}$ is measured body angular rates, $\overline{\omega}_b$ the body angular rates $\overline{\omega}_{SFCC}$ is a 3-by-3 matrix of scaling factors on the diagonal and misalignment terms in the non-diagonal, $\overline{\omega}_{bias}$ are the biases, (*Gs*) are the Gs on the gyroscope, and $\overline{\omega}_{gsens}$ are the g-sensitive biases.

2.3.3 Attitude Gyros

The attitude gyro is modeled as a first order filter. The output of the attitude gyros are limited to ±90° for pitch attitude, ±180° for roll and yaw attitudes.

$$\frac{\phi_s(s)}{\phi(s)} = \frac{\theta_s(s)}{\theta(s)} = \frac{1}{0.025s + 1} \quad (25)$$

2.3.4 The Compass Model

The compass model is shown in Figure 1, which consists primarily of two low pass filters.

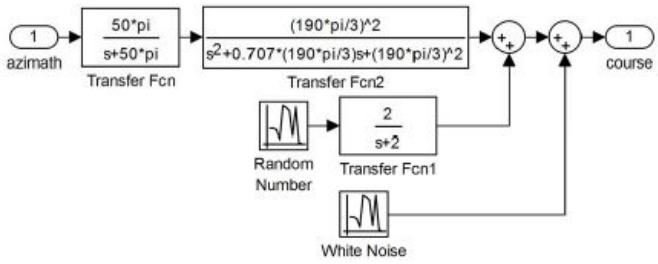

Figure 1: The compass model

2.3.5 Angle Of Attack Probe and Sideslip Vane

They are modeled as a simple filter which represent the probe and vane dynamics as:

$$\frac{\alpha_{probe}(s)}{\alpha(s)} = \frac{1}{0.073s+1} \quad , \quad \frac{\beta_{vane}(s)}{\beta(s)} = \frac{1}{0.073s+1} \tag{26}$$

2.3.6 Altitude and Velocity sensor

Pressure sensors are used for measuring the altitude and velocity, and are represented by a first order characteristic as:

$$\frac{H_s(s)}{H(s)} = \frac{1}{0.025s+1} \quad , \quad \frac{V_{Ts}(s)}{V_T(s)} = \frac{1}{0.03s+1} \tag{27}$$

2.3.7 GPS Modeling

A simple GPS position-velocity model includes output time-lag, Gauss-Markov noise correlation, and discrete output.

Conventionally, the longitudinal flight control system is designed for the longitudinal motion only; therefore the resulting linearized model is decoupled into longitudinal and lateral directional plants.

3. The Longitudinal Flight Controller

The longitudinal flight controller is realized using two control loops; altitude and velocity. The control system is implemented using two different controllers; PID with fixed gains tuned using Genetic Algorithm (GA), and the fuzzy logic control design technique.

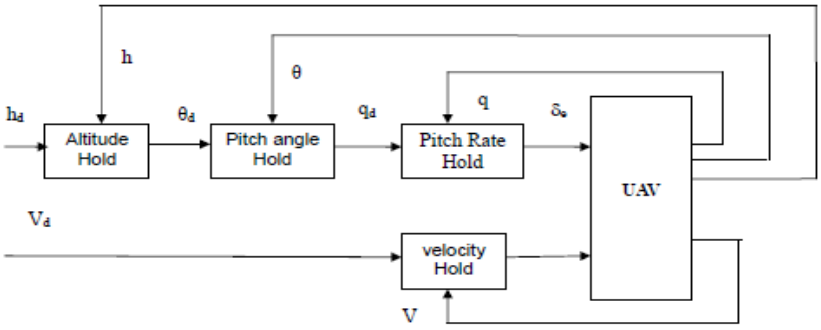

Figure 2: The longitudinal flight controller

3.1 Longitudinal classical PID controller

Initial guesses for the PID parameters are used then are optimized using a GA technique to improve the performance and robustness of the system. The transfer function of a PID controller is shown as:

$$G(s) = K_P + \frac{K_I}{S} + K_D S \tag{28}$$

Where: K_P, K_I, and K_D are the proportional, integral, and derivative gains respectively.

3.2 Longitudinal Fuzzy controller

A fuzzy logic controller system has two inputs, the error *e(t)* and change of error Δ*e(t)*, which are defined by:

$$e(t) = r - y \tag{29}$$

$$\Delta e(t) = e(t) - e(t-1) \tag{30}$$

The output of the Fuzzy Logic Controller is the incremental change in the control signal Δ*u(t)*. Then, the control signal is obtained by:

$$u(t) = u(t-1) - \Delta u(t) \tag{31}$$

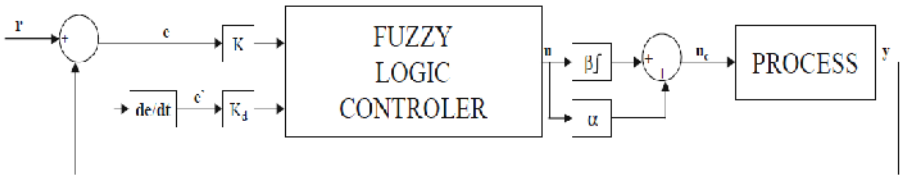

Figure 3: Fuzzy Logic Controller

4. Comparative Synthesis of UAV Flight Controllers

4.1 Reference tracking

The PID controller and the fuzzy controller are designed for the linearized model then is tested on a non-linear UAV model. Comparative synthesis of UAV flight controllers between the PID controller and the fuzzy controller is performed for specific altitude and speed commands as shown in the following figures. A step response of altitude with constant speed is shown as in Figure 4. The two controllers show almost identical responses, but the fuzzy controller yields better time response than the classical one.

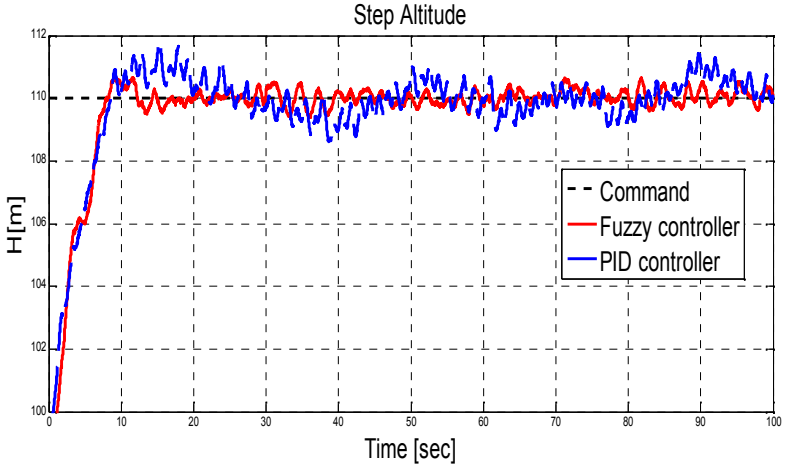

Figure 4: Step altitude

The speed response is affected instantaneously because of the coupling effect. A step response of speed with constant altitude is shown as in Figure 5. The two controllers show approximately identical responses, but also the fuzzy controller yields better time response than the classical one. The altitude response is slightly affected by speed change due to coupling effect.

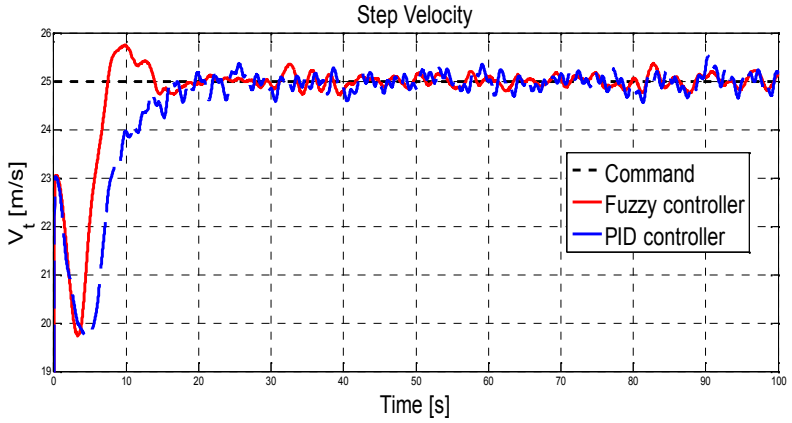

Figure 5: Step velocity

4.3 Effect of external wind disturbances

The effect of cross wind disturbance on the altitude and speed of UAV is shown in the following figures. The UAV is subjected to crosswind disturbance from the beginning of normal operation. If the wind speed exceeds certain limit, the PID controller provides better behavior than the fuzzy controller which has unstable response.

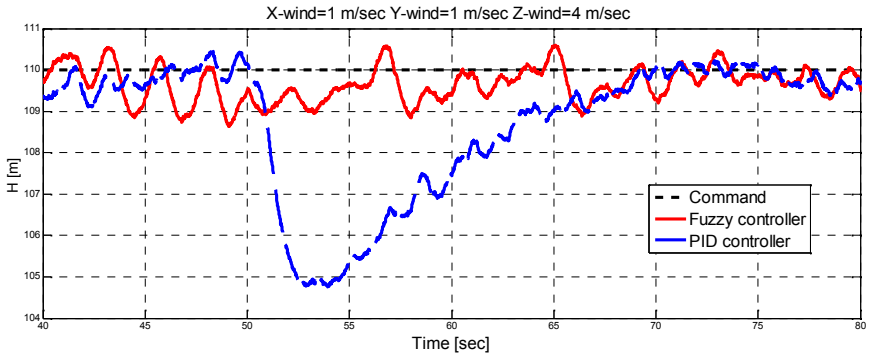

Figure.8: The Altitude response subjected to external wind disturbances.

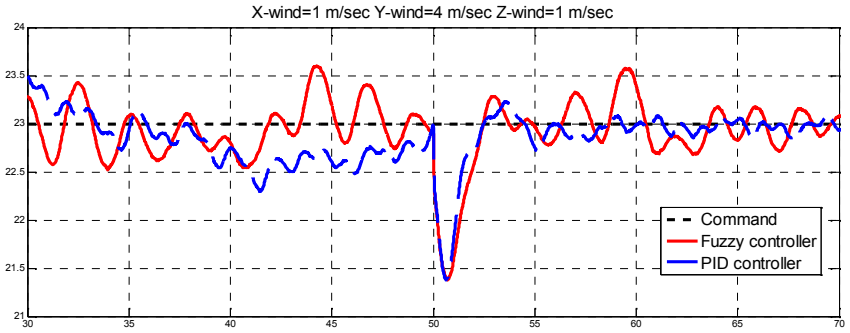

Figure.9: The velocity response subjected to external wind disturbances.

6-Conclusion

The nonlinear equations of motion for a non-rotating flat earth reference frame have been presented in this paper in a manner that they can be integrated into a simulation environment. The developed UAV model was simulated in MATLAB/Simulink using M-file for enhanced performance. Detailed models for the sensors and actuators were incorporated in the simulation. Comparative Synthesis of UAV flight controller between the optimized PID controller and the fuzzy controller has been presented for tracking step responses and the disturbance rejection.
Future work will focus on adjusting and validating the longitudinal controller so that it can be used to exploit the particular autopilot in its whole flight envelope. Extra effort will be placed on studying, developing, and testing advanced control strategies like adaptive control technique to achieve good performance characteristics in highly demanding maneuvers.

References

[1] Stevens, B.L. , F.L. Lewis, Aircraft Control and Simulation, John Wiley & Sons, 1992.
[2] Mileva,B., P. Boskoski, S. Deskoski, Fuzzy Logic Control of the Height of the Airplaine, 6th International PhD Workshop on Systems and Control, October 4-8, 2005 Izola, Slovenia.
[3] Christopher G., BS., Modeling, Simulation, and Flight Test for Automatic Flight Control of the Condor Hybrid Electric Remote Piltoed Aircraft,Thesis, AFIT/GSE/ENV/12-M04
[4] Jung,D., P.Tsiotras, Modeling and Hardware-in-the-Loop Simulation for a Small Unmanned Aerial Vehicle, Georgia Institute of Technology, Atlanta, GA, 30332-0150.
[5] PIO F. ,Flight Control System Design for Autonomous UAV Carrier Landing, PHD Thesis, Cranfield University, 2004.
[6] Salah I.,Application of Robust Control in Unmanned Vehicle Flight Control System Design, PhD Thesis, College of Aeronautics Cranfield University, 2003.
[7] Kortunov V.I., I.Yu. Dybska, G.A. Proskura & A.S. Kravchuk Integrated Mini INS Based on MEMS Sensors for UAV Control, IEEE A&E SYSTEMS MAGAZINE, JANUARY 2009.
[8] Hood River, OR 97031, Aerosim Blockset Version 1.2 User's Guide, http://www.u-dynamics.com.
[9] Sefer K., O. Çetin Autonomous Navigation and Landing Tasks for Fixed Wing Small Unmanned Aerial Vehicles, Acta Polytechnica Hungarica Vol. 7, No. 1, 2010
[10] Hector G., F. J. Pereda, J. M. Giron-Sierra,UAV Attitude Estimation Using Unscented Kalman Filter and TRIAD, IEEE TRANSACTIONS ON INDUSTRIAL ELECTRONICS, VOL. 59, NO. 11, NOVEMBER 2012
[11] Chao H., YongCan Cao, and YangQuan Chen, Autopilots for Small Unmanned Aerial Vehicles: A Survey, International Journal of Control, Automation, and Systems (2010) 8(1):36-44, DOI 10.1007/s12555-010-0105-z.
[12] Hong Y., W.K. Ho, A. Hansson, H. Hjalmarsson, J.W. Deng, Relay auto-tuning of PID controllers using iterative feedback tuning, Automatica 39 (2003) 149 – 157.
[13] Turkoglu K., Ugur Ozdemir, Melike Nikbay, and Elbrous M. Jafarov, PID Parameter Optimization of an UAV Longitudinal Flight Control System, World Academy of Science, Engineering and Technology 45 2008.
[14] Kurnaz s., O. Cetin · O, Kaynak, Fuzzy Logic Based Approach to Design of Flight Control and Navigation Tasks for Autonomous Unmanned Aerial Vehicles, the Journal of Intelligent and Robotic Systems, Volume 54, Nos 1–3, 229–244, Springer Science + Business Media B.V. 2008